

QM/MM Study of the Second Proton Transfer in the Catalytic Cycle of the D251N Mutant of Cytochrome P450cam

Muhannad Altarsha, Dongqi Wang,[†] Tobias Benighaus, Devesh Kumar, and Walter Thiel*

Max-Planck-Institut für Kohlenforschung, Kaiser-Wilhelm-Platz 1, D-45470 Mülheim an der Ruhr, Germany

Received: November 7, 2008; Revised Manuscript Received: May 20, 2009

Protonation of Compound 0 in the catalytic cycle of cytochrome P450cam may lead to the formation of either the reactive Compound I (coupling) or the ferric resting state (uncoupling). In this work, we investigate the effect of the D251N mutation on the coupling and uncoupling reaction by combined quantum mechanics/molecular mechanics (QM/MM) calculations. The mutated Asn251 residue has two possible orientations, i.e. directed toward the active site (no flip) or away from the active site (flip), with the latter one being preferred in classical molecular dynamics (MD) simulations. The possible proton transfer mechanisms in the coupling and uncoupling reaction were studied for three models of the D251N mutant, i.e. no flip (model I), flip (model II), and flip with an extra water (model III). According to the QM/MM calculations, the uncoupling reaction is always less favorable than the coupling reaction. The coupling reaction in the D251N mutant follows the same mechanism as in the wild-type enzyme, with initial O–O cleavage followed by proton transfer. The barrier for the initial step is similar in all D251N models, but the proton transfer is most facile in model III. The hydroxide anion formed in model III is not reprotonated easily by neighboring residues, while proton delivery from bulk solvent seems possible via a water network that remains intact during 2 ns classical MD simulation. The computational results are consistent with the experimental findings that the coupling reaction dominates the consumption of dioxygen in the D251N mutant, but with lower activity than in the wild-type enzyme.

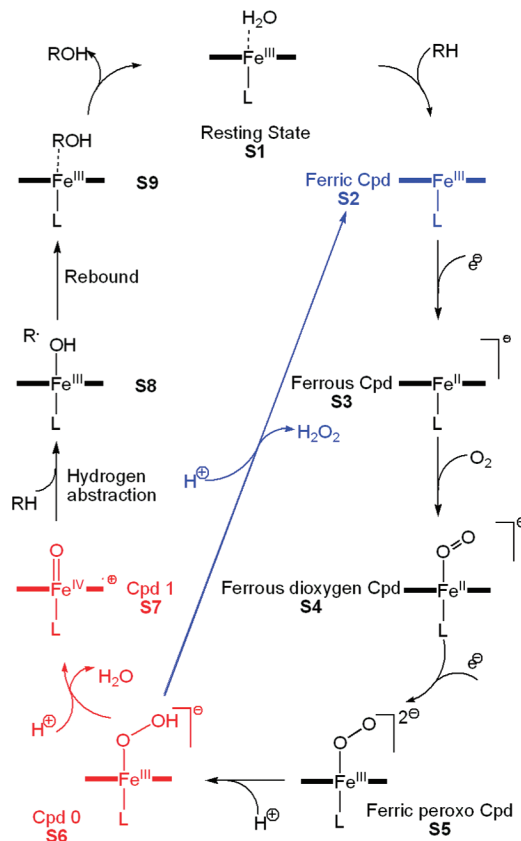
I. Introduction

Cytochromes P450 (P450s),¹ a ubiquitous family of heme containing monooxygenases, utilize dioxygen to insert an oxygen atom into inert hydrocarbon substrates. They play an important role in the biosynthesis of steroids, drug metabolism, and detoxification of xenobiotics.² Many studies of P450 have focused on the bacterial P450cam³ with a camphor substrate, the first soluble P450 protein whose sequence and X-ray structure were determined.⁴

The catalytic cycle of P450cam is shown in Scheme 1.³ The essential steps up to the formation of the active species involve (1) binding of the substrate, (2) reduction of the ferric cytochrome P450 to the ferrous state, (3) binding of molecular oxygen leading to the ferrous dioxygen complex, (4) second electron transfer and formation of the peroxy-iron(III) complex, (5) protonation of the distal oxygen, which leads to the formation of the ferric hydroperoxo complex (Compound 0, Cpd 0), and (6) second protonation of the distal oxygen with O–O bond cleavage, which generates the putative oxoferryl species (Compound I, Cpd I). Alternatively, protonation of the proximal oxygen in Cpd 0 leads to the uncoupling reaction that yields the ferric resting state and hydrogen peroxide instead of the hydroxylated product. Hence, a well-targeted proton transfer is indispensable for cleavage of the iron-bound dioxygen and formation of Cpd I.

Two proton delivery pathways have been proposed for P450cam that involve the highly conserved residues Asp251^{5–10} and Glu366.^{3,11,12} The crystallographic structure published by

SCHEME 1: Cytochrome P450cam Catalytic Cycle



523, and 902 (numbering as in PDB structure 1DZ8³), and the hydroxyl group of Thr252. The hydrogen bond network between the carboxyl group of Glu366 and the distal oxygen atom remains stable throughout molecular dynamics (MD) simulation.¹³ However, this chain terminates at Glu366 without any connection to the protein surface,¹⁰ and mutations of Glu366 show little influence on catalytic activity. These findings suggest that Glu366 does not play a major role in catalysis.^{9,10,14}

Closer inspection of the Asp251 channel renders this a better candidate. First, the crystallographic structure indicates that the Asp251 residue may serve as a proton shuttle between the solvent accessible Lys178/Asp182/Arg186 triad and Thr252.^{6,10,15,16} This is supported by MD simulations that confirm the flexibility of the Asp251 residue.^{17–19} Second, extensive site-directed mutation studies clearly indicate that Asp251 and Thr252 play a vital role in the catalytic cycle.^{6,10,20,21} Therefore, it has been suggested that the Asp251 and Thr252 residues are important in constituting a controlled proton delivery pathway that involves solvent water and provides an active-site H-bond donor. This may be a trapped water molecule or Thr252.^{6,10}

An alternative proposal²² assumes that the proton transfer from the solvent into the active site of P450 may proceed through the hydration cluster close to the heme propionates in the resting state. However, after the entry of the substrate, this pathway is blocked and will therefore not be considered.³

The D251N mutation causes a structural change in the vicinity of the active site. The new Asn251 amide side chain no longer favors the hydrogen bonds with Thr185 and Lys178 that keep Asp251 in an orientation toward the active site. Instead, Asn251 forms a new hydrogen bond with Asp182 and rotates away from the active site. This makes the active site more accessible for the solvent, such that an alternative solvent-based proton delivery channel may be established, as indicated by solvent kinetic isotope effect measurements.^{4,10} Overall, the D251N mutant exhibits a greatly diminished rate of O₂ consumption for the coupling reaction. The product formation rate decreases by a factor of more than 30 from 820 nmol/min/nmol heme in the wild-type enzyme to 26 nmol/min/nmol heme in the D251N mutant; this has been interpreted in terms of a slower proton transfer to the iron-linked dioxygen.¹⁰

Mutation of the Thr252 residue by amino acids without hydrogen-bonding side chains virtually suppresses camphor hydroxylation in favor of the uncoupled reduction of O₂ to H₂O₂.^{5,8,10,23} The crystal structure of the pentacoordinated ferric complex of the Thr252Ala mutant indicates that the solvent may be responsible for the observed uncoupling of the enzyme turnover from camphor hydroxylation in this mutant, since it contains a water molecule near the O₂ binding site, which is not present in the wild-type enzyme.^{11,23}

Although the formation of Cpd I from Cpd 0 has been the subject of numerous theoretical studies, their results were partly inconsistent and mechanistic details such as the stability of a protonated Cpd 0 intermediate (prot-Cpd 0) depended strongly on the chosen model system.^{11,17,24–28} Therefore, Zheng et al.¹⁹ studied the formation of Cpd I in the full P450cam enzyme using a hybrid quantum mechanical/molecular mechanical (QM/MM) approach. They found that protonated Cpd 0 is an intermediate only in the Glu366 channel. It is very high in energy (more than 20 kcal/mol above Cpd 0) and the barrier for its decay is only 3–4 kcal/mol toward either Cpd 0 or Cpd I. In the Asp251 channel, protonated Cpd 0 was found to be unstable. Therefore, a novel mixed homolytic–heterolytic mechanism was proposed as the most favored pathway in both channels,¹⁹ with the rate-limiting step being the initial O–O

bond cleavage with a barrier of about 13–14 kcal/mol. The same methodology was used to study the effect of mutations at the Thr252 position to explain the important role of this residue in the proton delivery pathway and to rationalize the preference for coupling or uncoupling in the Thr252 mutants.²⁹

Wang et al.³⁰ compared the role of the Asp251 and Asn251 residues during formation of Cpd 0 in the wild-type enzyme and the D251N mutant, respectively. In the D251N mutant, the Asn251 side chain was observed to be flexible during MD simulations and to flip from an orientation toward the active site to an orientation away from the active site, which generates some empty space between Arg186 and Wat901 that may be filled by an extra water molecule. QM/MM calculations on the resulting no flip, flip, and flip with extra water models led to the conclusion that the proton transfer in the Asn251 channel requires either a back-flip of the Asn251 side chain or the participation of an extra water molecule in the active site, and even then the barriers are higher than those in wild-type P450cam.

Until now, the effect of the D251N mutation on the coupling and uncoupling reactions of Cpd 0 has not been studied by QM/MM methods that account for the full enzyme. This article reports QM/MM calculations on both reaction pathways for the D251N mutant and the wild-type enzyme to elucidate the mechanistic role of the Asp251 residue and solvent molecules. In section II we briefly describe the computational methods employed. In section III we present and discuss the results of classical MD simulations and of QM/MM calculations for the different D251N models and compare them to results for the wild-type enzyme and to experimental data. Finally, section IV offers conclusions.

II. Computational Methodology and Proposed Mechanisms

QM/MM Setup. The available experimental X-ray structure of cytochrome P450cam (PDB code, 1DZ8;³ resolution, 1.9 Å) was used as a starting point in our work. The same protonation and solvation protocol was employed as in previous studies.^{31–33} Glu366 remains deprotonated, since we do not consider the Glu366 channel. Asn251 is neutral in the D251N mutant while Asp251 was protonated in our related previous QM/MM work on the wild-type enzyme.^{19,30}

Both the wild-type and mutant system contain around 25000 atoms including 5895 TIP3P water molecules.³⁴ The initially prepared systems were relaxed by energy minimizations and MD simulations using the CHARMM22 force field³⁵ as implemented in the CHARMM program.³⁶ During the MD simulation, the heme unit, Cys357, and the outer 8 Å of the solvent layer were kept fixed.

The chosen QM/MM methodology is analogous to that used in previous studies.^{19,30–33} Therefore, only those aspects relevant to the present work are mentioned here. Minimized snapshots from classical MD simulation trajectories were taken as the initial structures for QM/MM calculations. The QM region was described by unrestricted hybrid DFT (UB3LYP)³⁷ using the LACVP³⁸ small-core ECP basis set on Fe and 6-31G³⁹ on the rest of all atoms (B1) for geometry optimizations. Single-point calculations were carried out with the TZVP^{40,41} basis set (B2) applied to all atoms. The CHARMM force field was run through the DL_POLY⁴² code to treat the MM part of the system. All QM/MM calculations were performed with the ChemShell package⁴³ that integrates the TURBOMOLE⁴⁴ and DL_POLY programs and also provides the HDLC optimizer⁴⁵ for geometry optimizations. An electronic embedding scheme⁴⁶ was adopted

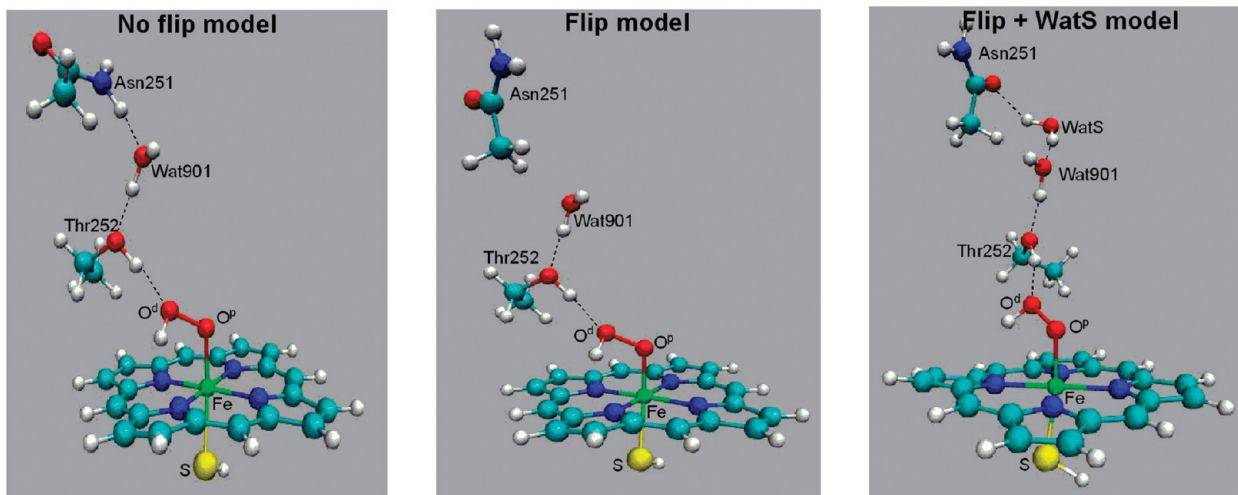
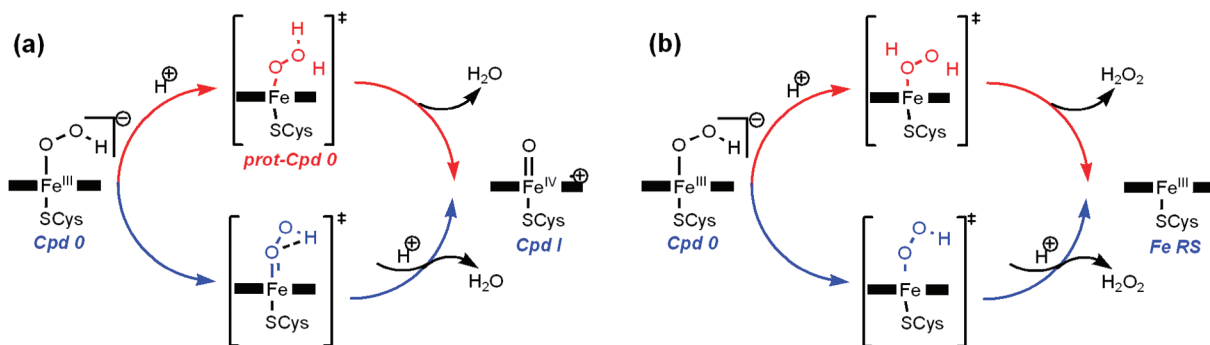


Figure 1. QM models for the Asn251 mutant: Model I represents the no flip configuration of the Asn251 side chain, model II represents the flip configuration, and model III extends model II with an extra water molecule (WatS).

SCHEME 2: (a) Two Proposed Reaction Mechanisms for Cpd I Formation (Coupling Reaction), and (b) Two Proposed Reaction Mechanisms for Ferric Resting State Formation (Uncoupling Reaction)



in the QM/MM calculations; that is, the MM charges were included in the one-electron Hamiltonian of the QM part, and QM/MM electrostatic interactions were evaluated as interaction of the QM electrostatic potential with MM partial charges. Hydrogen link atoms in combination with a charge shift model⁴⁷ were employed to treat the QM/MM boundary. All minima (reactants, products, and intermediates) and transition states (TS) reported in this paper were fully optimized.

The active region was defined to include all residues and water molecules within 6 Å of any non-hydrogen atom of the core region which contains the heme unit, Cys357, Glu366, Asn251, Thr252, Wat523, Wat566, Wat687, Wat901, and WatS. This results in ca. 1400 atoms to be optimized.

QM Region. We used an analogous QM region as in previous work on the wild-type enzyme.¹⁹ In the D251N mutant, the Asp251 residue was manually replaced by Asn, and the QM region thus includes the following: porphyrin-FeOOH without side chains, SH ligand, Asn251 (CH_2CONH_2), Thr252 (CH_3CHOH), and Wat901. This QM region is shown in Figure 1 for models I and II, which represent the no flip and flip conformations encountered during 2 ns classical MD simulations (see below). In model III an extra water molecule (WatS) was manually placed in the empty space between Arg186 and Wat901. The stability of WatS in the active site was confirmed by means of classical MD simulation, and therefore, model II was extended to model III by including WatS. The three models are illustrated in Figure 1.

Possible Proton Transfer Pathways. Scheme 2 presents possible pathways that yield two different products through

proton transfer, respectively. In the first two pathways (coupling reactions, Scheme 2a), the proton is transferred from the hydroxy group of threonine to the distal oxygen (O^d), while in the other two pathways (uncoupling, Scheme 2b), the proton is transferred to the proximal oxygen (O^p). In both cases, Wat901 bridges Asn251 and Thr252 (and WatS in model III) to construct the proton transfer channel. The details of these mechanisms are as follows.

In the coupling reaction (Scheme 2a), which leads to the formation of Cpd I and one water molecule, the proton is transferred to the proximal oxygen atom of the O_2H moiety and protonated Cpd 0 is formed, followed by a heterolytic O–O bond cleavage that yields Cpd I and water.¹⁹ In the second mechanism, an initial O–O bond cleavage generates an OH species hydrogen-bonded to the FeO moiety. A subsequent proton transfer to this OH species with a concomitant electron transfer from the heme yields Cpd I and water¹⁹ (blue pathway in Scheme 2a).

The uncoupling reaction (Scheme 2b) leads to the formation of the ferric resting state and hydrogen peroxide. Two possible mechanisms have been investigated also for this reaction. The first one (red pathway in Scheme 2b) starts with a proton transfer to the proximal oxygen to form $\text{Fe}-\text{O}_2\text{H}_2$, followed by heterolytic Fe–O bond cleavage that generates the ferric resting state and hydrogen peroxide. In the second mechanism, the

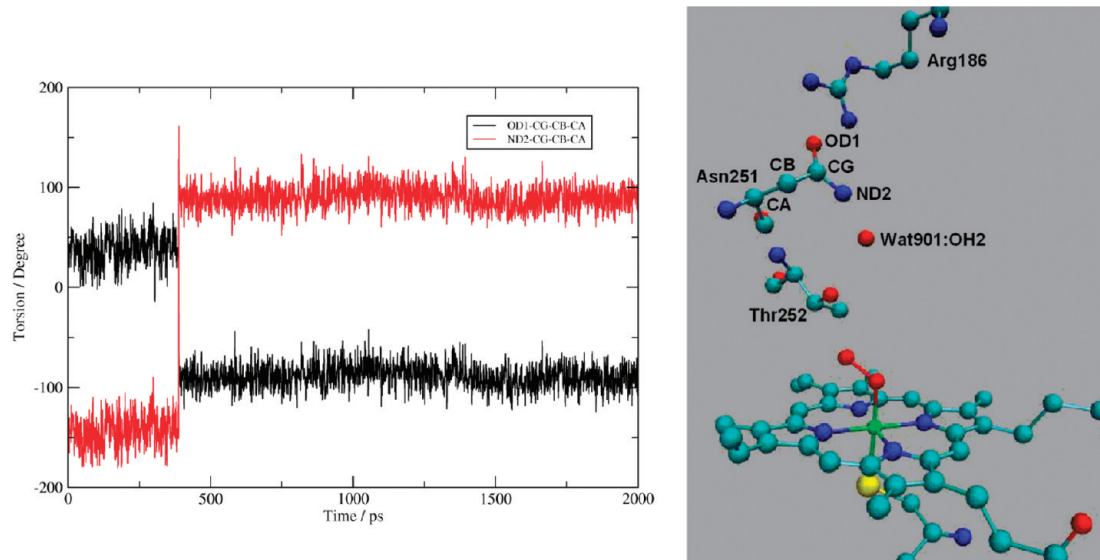


Figure 2. Motion of the Asn251 side chain during the MD simulation. Left: results for torsion angles OD1–CG–CB–CA and ND2–CG–CB–CA. Right: definition of atom labels.

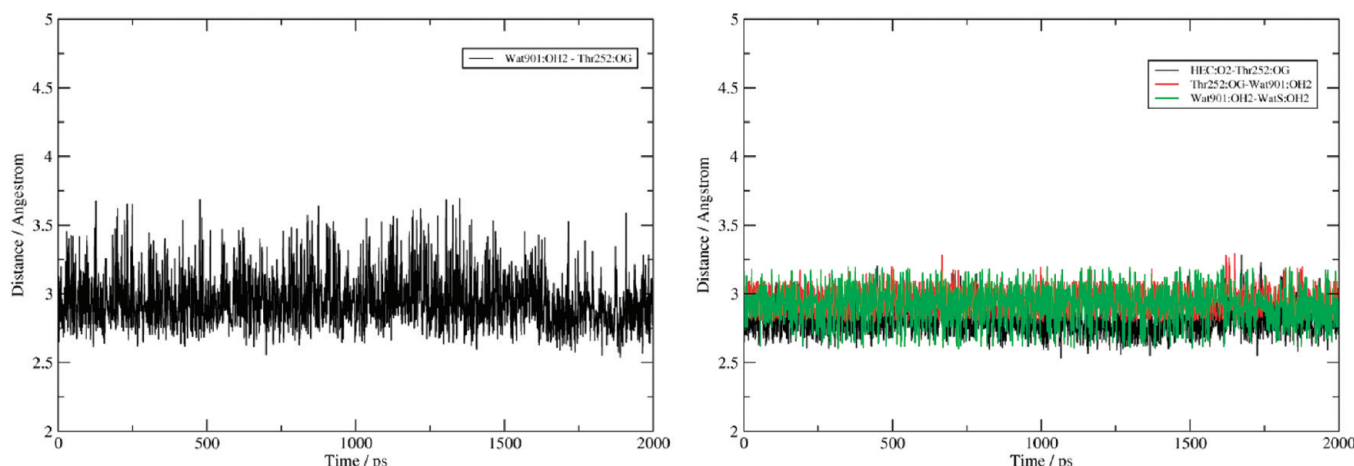


Figure 3. Monitoring the mobility of the crystallographic water molecule (Wat901) and the extra water molecule (WatS) during the MD simulation (for atom labels, see Figure 2). Left: Wat901 in model II. Right: Wat901 and WatS in model III.

Fe–O bond is cleaved first and a hydroperoxo radical is formed, which is then converted to hydrogen peroxide.

III. Results and Discussion

MD Simulation Results. The crystal structure of the D251N mutant (2A1N)⁴⁸ is a dimer which contains the Asn251 residue in two different orientations in the two units (normal and flipped orientation). In the former case, the Asn251 side chain shows a 25° rotation toward Wat901, thus establishing a connection to the active site.⁴⁸ This suggests that there is no strong interaction between Asn251 and Arg186, unlike the salt bridge which exists between Asp251 and Arg186 in the crystal structure of the wild-type enzyme (1DZ8). Consequently, a direct interaction between Asn251 and Wat901 is possible, and a proton transfer channel from Asn251 via the only crystallographic water molecule in this region (Wat901) to the active site may be formed.^{10,18}

We performed a 2 ns classical MD simulation of the D251N mutant of Cpd 0 starting from model I (no flip) to study the stability of the Asn251 amide group. Its conformation is characterized by two torsion angles with the backbone (OD1–CG–CB–CA and ND2–CG–CB–CA). During the simulation (see Figure 2), the OD1–CG–CB–CA torsion angle

decreases from 70° to –90°, whereas the ND2–CG–CB–CA angle increases from –108° to 88°. In the no flip conformation, the Asn251 residue forms hydrogen bonds with nearby residues, i.e. Arg186 and Wat901 (relevant average distances: Arg186:HH22–Asn251:OD1, 1.809 Å; Arg186:HH12–Asn251:OD1, 1.779 Å; Wat901:OH2–Asn251:HD22, 1.656 Å). After the flip of the Asn251 side chain (model II), the amide group of Asn251 retains its hydrogen bond with Arg186 and forms new hydrogen bonds with Thr181 and Asp182 (average distances: Thr181:OG1–Asn251:HD22, 2.049 Å; Asp182:OD1–Asn251:HD21, 1.651 Å).

Wat901 and WatS play a critical role in the proton delivery, and we have therefore checked their mobility by additional MD simulations. Figure 3 shows the results for Cpd 0 in model II (left) and model III (right). The connection between Wat901 and the side chain of Asn251 is interrupted in model II (flip) of the Asn251 mutant. However, since Wat901 keeps its hydrogen bond with the Thr252:OH group, it does not escape from the protein pocket during the 2 ns simulation but stays close to Thr252 (see Figure 3). Likewise, in model III (flip with extra water), Wat901 remains stable next to the Thr252 amino acid: the average value and the standard deviation for the distance between Wat901:OH2 and Thr252:OG1 is 2.955 ± 0.224 Å,

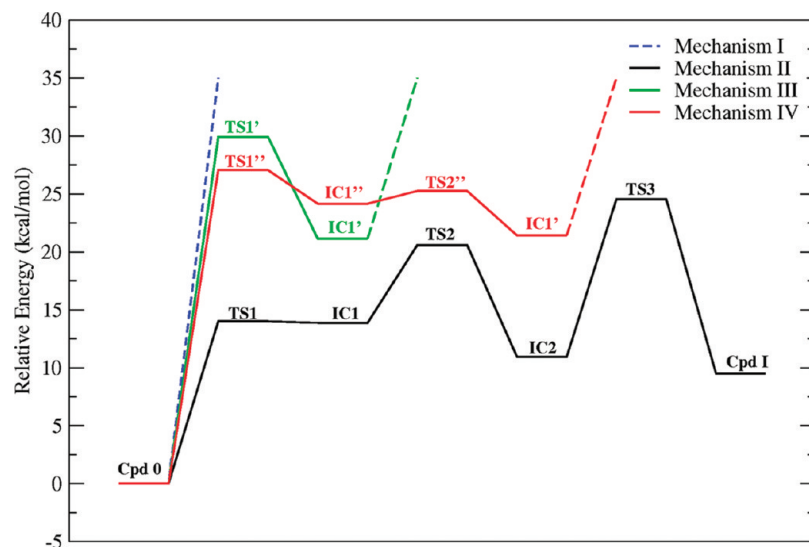


Figure 4. Energy profiles for the four possible mechanisms in the no flip conformation of the D251N mutant (I and II for coupling, III and IV for uncoupling). Relative energies are given in kcal/mol with respect to Cpd 0.

indicating that the hydrogen bond between Thr252 and Wat901 is conserved. The extra water molecule that is inserted in model III (WatS) does not escape from the distal pocket during the MD simulation: the average value and the standard deviation for the distances HEC:O2–Thr252:OG1, Thr252:OG1–Wat901:OH2, and Wat901:OH2–WatS:OH2 are 2.803 ± 0.102 Å, 2.940 ± 0.096 Å, and 2.925 ± 0.127 Å, respectively. These results confirm that both water molecules are stable in the distal pocket of the enzyme.

QM/MM Results. In the following, we present the results from QM/MM geometry optimizations and reaction path calculations for models I–III. Since previous work on the native enzyme and several mutants has established that the doublet state of Cpd 0 is more stable than the quartet state both in gas phase models^{7,26} and in the actual enzyme environment,¹⁹ we focus on the doublet spin state in this study. The QM/MM optimized structures of the QM region of the D251N mutant have already been shown in Figure 1 for Cpd 0 in models I–III. The figures in this section will present QM/MM optimized structures of all relevant stationary points (with data for selected geometrical parameters) as well as energy profiles (with relative energies obtained from the B1/B2 basis sets). Since the computed relative energies are not too sensitive to extension of the basis set, we shall discuss the B1 values in the text (B1 is the basis used for geometry optimization). Other computational results (such as spin densities, Mulliken charges, and additional reaction profiles) are documented in the Supporting Information (SI), which also provides an overview picture of the active-site structure (Figure S38).

A. No Flip Model. As already mentioned, four different reaction mechanisms were studied for the coupling and uncoupling reactions of Cpd 0. The coupling mechanisms I and II yield Cpd I and water, while the uncoupling mechanisms III and IV lead to the formation of the ferric resting state and hydrogen peroxide. Figure 4 shows the energy profiles of all mechanisms for the no flip model. In the case of mechanism I (blue line in Figure 4), the energy profile goes uphill only, and we were unable to locate a stable prot-Cpd 0 intermediate. In previous QM/MM studies by our group on the native enzyme and the Thr252X (X = Ser, Ala, Val, Gly) mutants in the Asp251 channel, prot-Cpd 0 was also found to be unstable.^{19,29} Mechanism II proceeds in three steps (black line in Figure 4). The first one is O–O bond cleavage with an energy barrier of

14.0 kcal/mol. In the second step, the hydrogen on Thr252 is transferred to the OH moiety with an energy barrier of 8.0 kcal/mol followed by the deprotonation of Asn251 with a barrier of 13.6 kcal/mol relative to IC2.

In contrast to mechanism II, mechanisms III and IV give the ferric resting state and hydrogen peroxide. Mechanism III (green line in Figure 4) starts with a direct proton transfer from the Thr252 residue to the proximal oxygen (O1) of the FeOOH moiety, accompanied by a spontaneous O–Fe bond cleavage. This step has an energy barrier of 29.9 kcal/mol. After this proton transfer, the first intermediate (IC1'), comprising the ferric resting state and hydrogen peroxide with an O-Thr252 anion, is calculated to be 21.1 kcal/mol above the reactant. The recovery of the natural state of Thr252 by abstracting a proton from Asn251 seems to be unrealistic in this model, since deprotonated Asn251 is a significantly stronger base than deprotonated Thr252 in IC1'. Therefore, the proton channel is interrupted and this mechanism does not lead to the desired product.

In mechanism IV (red line in Figure 4), the initial step is O–Fe bond cleavage with a barrier of 27.1 kcal/mol. The resulting intermediate IC1'' contains an OOH moiety and has an energy of ca. 24 kcal/mol. In the next step, a proton is transferred from Thr252 to the proximal oxygen of the OOH moiety with a tiny barrier of only around 1 kcal/mol relative to IC1''. This step leads to an intermediate that is very similar to the one of mechanism III and has an energy of 21.4 kcal/mol. However, in mechanism IV the product of the final proton transfer from Asn251 to the deprotonated Thr252 is again not stable.

In summary, we find that mechanism I is not a realistic pathway, since the formation of its first intermediate (prot-Cpd 0) is difficult. Mechanisms III and IV involve significantly higher activation energies than mechanism II already in the initial stage of the reaction. Qualitatively similar results were also obtained for models II and III. Hence, mechanism II emerges as the most favorable pathway, and we will discuss only this mechanism in detail for all three models. Further information about the other mechanisms is given in the Supporting Information.

Figure 5 presents the QM/MM optimized structures and the energy profile of mechanism II in the no flip model of the D251N mutant. In this conformation, the hydrogen bonding

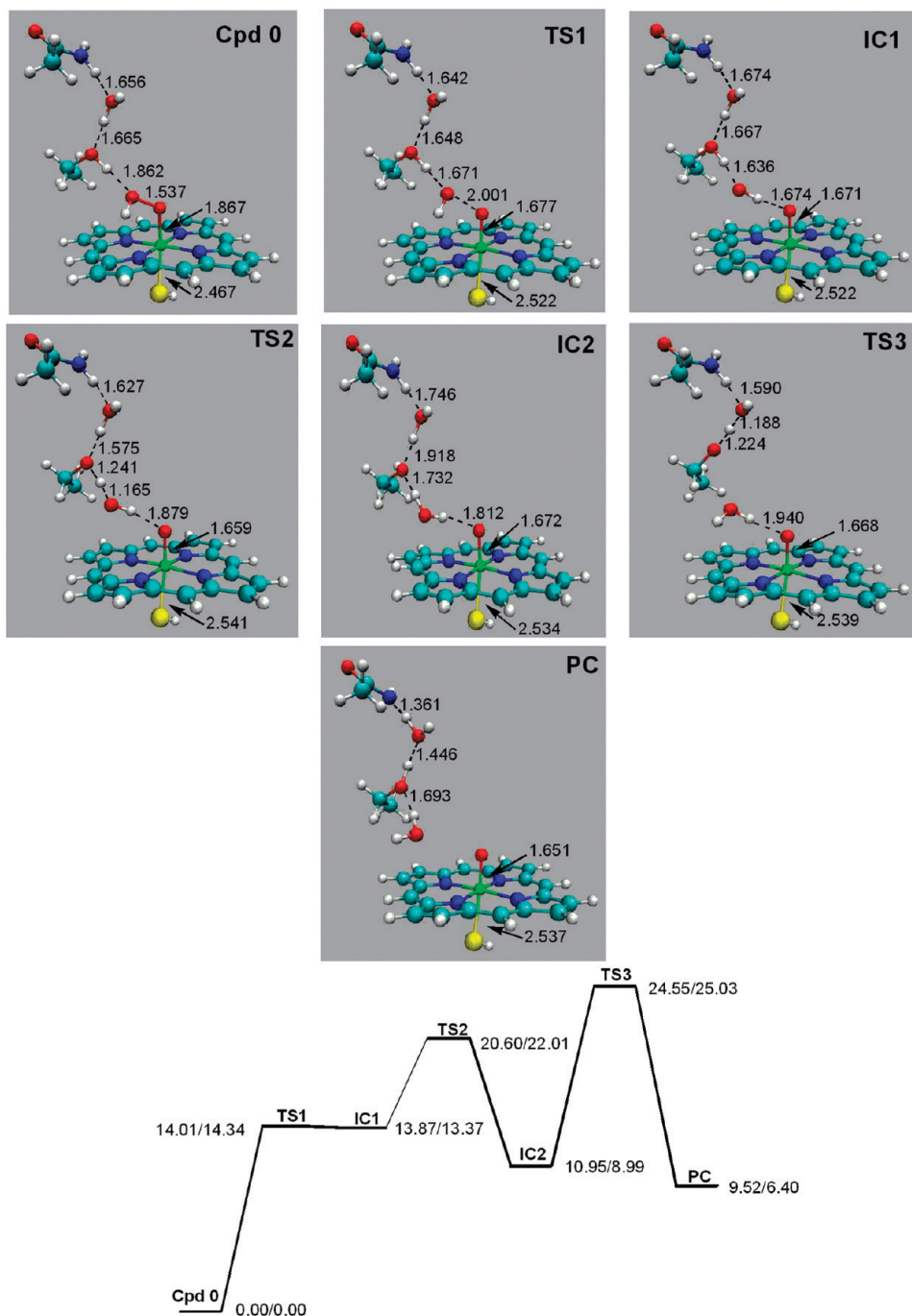


Figure 5. Asn251 mutant, no flip model. (a) Optimized geometries of Cpd 0, TS1, IC1, TS2, IC2, TS3, and PC (UB3LYP/B1/CHARMM). Only the QM region is shown. (b) Energy profile of mechanism II. Energies in kcal/mol relative to Cpd 0 (B1/B2).

network between the proton source (Asn251) and the distal oxygen (O^d) is conserved. The O^d-O^p bond cleavage has a barrier of 14.0 kcal/mol (i.e., very similar to the wild-type enzyme) and leads to the first intermediate (IC1) with an energy of 13.9 kcal/mol. During the first step, the O^d-O^p distance increases from 1.537 (Cpd 0) to 2.001 (TS1) and 2.524 Å (IC1), indicating cleavage of the O–O bond. Meanwhile, the Fe– O^p distance decreases noticeably from 1.867 to 1.677 Å from reactant to first transition state, and the Fe–S distance elongates from 2.467 (Cpd 0) to 2.522 Å (TS1, IC1).

During the reaction, the hydrogen bond between Thr252 and the distal oxygen atom becomes stronger due to the displacement of the OH moiety toward the Thr252 residue. In IC1, a new strong FeO–HO hydrogen bond with a distance of 1.674 Å is formed. The spin density and charge of the OH moiety in IC1

are –0.7 and –0.1, respectively, which indicates that OH will not behave as a “perfect” radical in IC1. This is due to the strong hydrogen-bonding interactions of the OH moiety with both the heme (through FeO) and the protein environment (through Thr252). A similar spin density was reported previously for the wild-type enzyme.¹⁹

The subsequent proton transfer from Asn251 to the distal oxygen proceeds in two steps. First, a hydrogen atom is transferred from Thr252 to the OH moiety, and then Thr252 is reprotonated via Wat901 by Asn251 with a concomitant electron transfer from the heme. During the first step, the system has to pass over a high energy barrier (TS2) of 20.6 kcal/mol to reach a stable intermediate (IC2) with an energy of 11.0 kcal/mol. In IC2, the spin density of the OH group reduces to almost zero and the hydrogen atom of Thr252 is transferred to the distal

oxygen (0.997 \AA) to form a water molecule. The spin density and Mulliken charge on Thr252 are -1.0 and -0.2 , respectively. The radical character of Thr252 in IC2 is confirmed by QM/MM calculations with different QM regions, functionals, basis sets, and initial guesses for the density matrix (see Tables S27–S29 of the Supporting Information). The occurrence of such an IC2 radical intermediate in the D251N mutant contrasts with the situation in the wild-type enzyme where the proton transfer from Asp251 is more facile (due to the much higher acidity of Asp251 compared with Asn251) and proceeds in a concerted manner. The transition state of the last step (TS3) in the mutant has an energy of 24.6 kcal/mol above Cpd 0, representing the highest point of the whole pathway. The overall process is endothermic by 9.5 kcal/mol . Reaction path calculations indicate that a concerted proton transfer in the mutant requires an activation of about 39 kcal/mol relative to Cpd 0 (see the Supporting Information).

It is also worthwhile to discuss the nature of IC1 and TS1. In a previous study that employed the same model of the wild-type enzyme, we found a similar reactive high-energy species whose stability depends on the size of the QM region.¹⁹ In view of the energetic similarities of TS1 and IC1 (IC1 is about 0.2 kcal/mol more stable than TS1) and the geometric similarities of IC1 and TS2, it seems probable that TS1 and IC1 are artifacts resulting from the limited size of the QM region and the absence of conformational sampling. Hence, it is more realistic to regard the no flip mechanism in the mutant as a two-step process. The first step then corresponds to O–O bond cleavage, hydrogen transfer, and water formation with an overall barrier of 20.6 kcal/mol . The second step is the deprotonation of the mutated Asn251 residue with a barrier of 13.6 kcal/mol .

The major difference between the wild-type enzyme and the D251N mutant is 2-fold: (1) The barrier of the rate-determining step increases from 14.4 kcal/mol in the wild-type enzyme to 20.6 kcal/mol in the D251N mutant. (2) The formation of Cpd I is a one-step process in the wild-type enzyme, while it becomes a two-step reaction in the D251N mutant with a stable deprotonated Thr252 radical intermediate. Both effects result from the much higher pK_a value of the mutated Asn251 residue compared to Asp251 that acts as the proton source in the wild-type enzyme.

Finally, we tested if an extension of the QM region has a significant effect on the relative energies by including the Arg186 residue into the QM region. We found only very minor changes in relative energies and geometries (see the Supporting Information).

B. Flip Model. In the flipped conformer, rotation of the Asn251 residue causes an interruption of the hydrogen bond network so that it cannot serve as a proton source. Figure 6 shows the QM/MM optimized structures with selected geometric parameters and the energy profile of mechanism II in the flip model. The first step, cleavage of the O–O bond, remains unaffected by the Asn251 flip: the transition state (TS1) and the first intermediate (IC1) have energies of 14.0 and 9.0 kcal/mol relative to Cpd 0, respectively. The spin densities of OH (-1.0) and Fe=O (2.1) in IC1 indicate that the Fe=O moiety carries two unpaired electrons, and the third unpaired electron is mainly located at the OH moiety. The hydrogen bond interactions with the proximal oxygen of the heme and Thr252 that stabilize the OH radical are structurally similar to those of model I but provide a more efficient energetic stabilization of ca. 5 kcal/mol (relative to TS1). Subsequently, the reaction follows a radical mechanism as in the no flip model. The second step is the hydrogen transfer from Thr252 to the OH radical

with a transition state (TS2) energy of 17.6 kcal/mol and an intermediate complex (IC2) at 12.4 kcal/mol . The computed spin densities and charges confirm that the proton transfer leads to the formation of a water molecule and the O-Thr radical species (see Tables S6 and S28 of the Supporting Information). Finally, a proton from water (Wat901) and an electron from the heme are transported to the O-Thr252 radical. The corresponding transition state (TS3) and the product complex lie 21.1 and 19.2 kcal/mol above Cpd 0, respectively.

The resulting product complex contains a negatively charged OH species with weak radical character, as indicated by the computed spin density and Mulliken charge (-0.2 and -0.5 , respectively). This species is stabilized by strong hydrogen bonds with Thr252 and Asn251 (distances of 1.427 and 1.888 \AA , respectively). The reaction pathway is blocked at this stage, since the Asn251 residue does not act as a proton source in the flip model and no other proton source exists in the vicinity. We have also included the Arg186 side chain into the QM region to check if Arg186 may serve as an alternative proton source but found that the distance to the OH anion is too large to enable proton transfer (details see in the Supporting Information). We thus have to conclude that flip conformations of this kind are unlikely to contribute to the formation of Cpd I in the D251N mutant.

C. Flip Model with an Extra Water WatS. As mentioned before, an extra water fits into the space which is released by the flip of the Asn251 side chain (see Figure 1). The introduction of WatS improves the hydrogen bond network with the Arg186 residue that is a potential proton source. Figure 7 presents the QM/MM optimized geometries and the energy profile for the flip model in the presence of the WatS molecule. In this pathway, the O^d–O^p bond cleavage has an energy barrier of 14.0 kcal/mol , similar to cases of the no flip and flip models. The energy of the first intermediate complex (IC1) is 11.8 kcal/mol relative to that of Cpd 0. The spin densities and Mulliken charges of the OH group and the proximal oxygen atom also confirm the cleavage of the O–O bond. The OH group in IC1 forms two strong hydrogen bonds with the heme and the Thr252 residue (distances of 1.447 and 1.690 \AA , respectively).

The energy barrier of the second step which involves proton transfer from Wat901 to the OH moiety via Thr252 and concomitant electron transfer from the heme is 0.3 kcal/mol . The whole reaction is endothermic, with the product lying 7.7 kcal/mol above Cpd 0. Both the OH spin density (-0.2) and Mulliken charge (-0.5) indicate that an anionic OH species with only weak radical character is formed, which is stabilized by two hydrogen bonds with Thr252 and WatS (distances of 1.236 and 1.638 \AA , respectively). Evidently, the proton transfer is facilitated by the additional water molecule, and the overall endothermicity decreases from 19.2 kcal/mol in model II to 7.7 kcal/mol in model III. Since the barrier for proton transfer is reduced to less than 0.5 kcal/mol , it is appropriate to regard the overall process essentially as a one-step reaction similar to model I.

Starting from the product complex, we tried to move one proton from WatS to the OH anion of Wat901. However, this proton always moved back to the emerging hydroxide anion upon full QM/MM optimization, indicating that WatS is an even weaker Brønsted acid than Wat901 in the given environment (see SI for detailed information). Closer inspection of these structures indicates that WatS also forms a hydrogen bond with the Arg186 residue, thus making Arg186 a potential proton source. To explore the role that Arg186 plays in the presence of WatS, we included the side chain of the Arg186 residue into

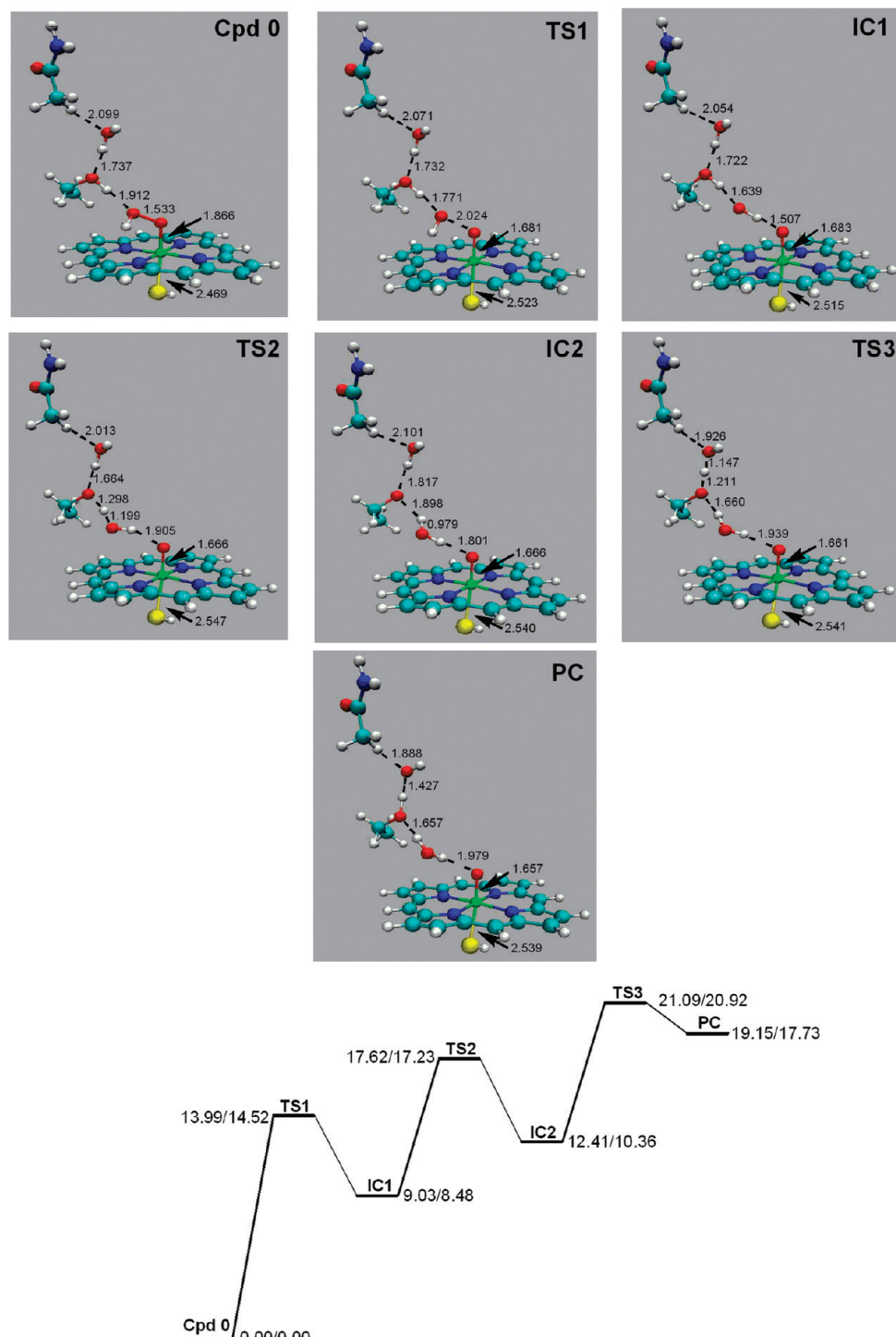


Figure 6. Asn251 mutant, flip model. (a) Optimized geometries of Cpd 0, TS1, IC1, TS2, IC2, TS3, and PC (UB3LYP/B1/CHARMM). Only the QM region is shown. (b) Energy profile of mechanism II. Energies in kcal/mol relative to Cpd 0 (B1/B2).

the QM region and tested if it can act as a proton source. Figure 8 presents the QM/MM optimized geometries of the reactant, first intermediate, and product complex of the flip model with an extra water molecule and Arg186 included in the QM region. The product complex (PC) contains an OH anion (Wat901) that is stabilized by strong hydrogen bonds to Thr252 (1.334 Å) and Wat901 (1.549 Å). We tried to locate the alternative product complex (PC') with deprotonated Arg186 and two water molecules that would be formed by proton transfer from Arg186 to the OH anion (Wat901). However, constrained geometry optimizations indicate that PC' is less stable than PC by about 8 kcal/mol and that the rearrangement from PC' to PC is

barrierless. This implies that in the given environment Wat901 is a better proton donor than Arg186 due to the favorable stabilization of the formed OH anion through hydrogen bond interactions. We have to conclude that deprotonated Wat901 will not be replenished by proton transfer via Arg186.

Further inspection of the structure of the product complex (PC) reveals that the hydroxide anion of Wat901 may be connected to the bulk solvent via WatS and three crystallographic water molecules (Wat149, Wat148, and Wat133) and that this network can further be improved by including an additional water molecule in the vacant space between WatS and Wat149. We have confirmed that this extended water

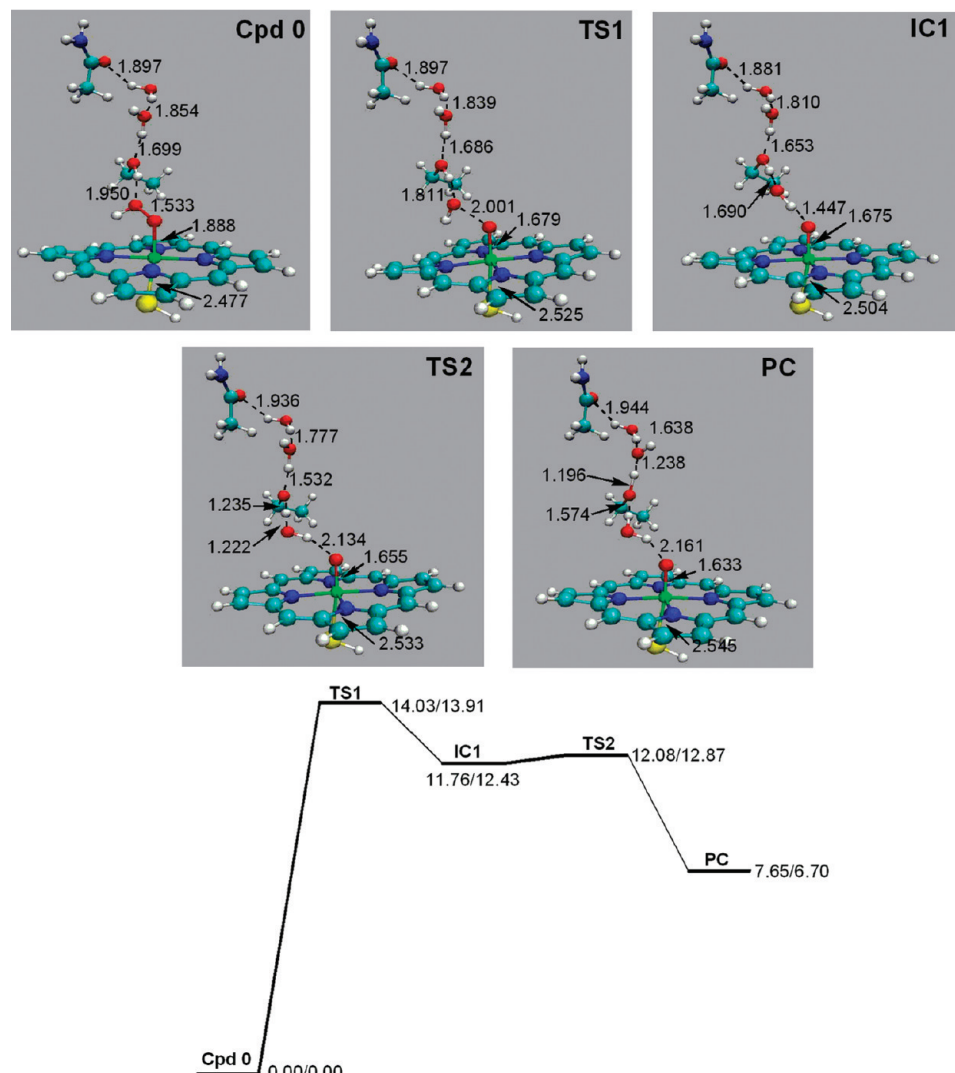


Figure 7. Asn251 mutant, flip model with an extra water. (a) Optimized geometries of Cpd 0, TS1, IC1, TS2, and PC (UB3LYP/B1/CHARMM). Only the QM region is shown. (b) Energy profile of mechanism II. Energies in kcal/mol relative to Cpd 0 (B1/B2).

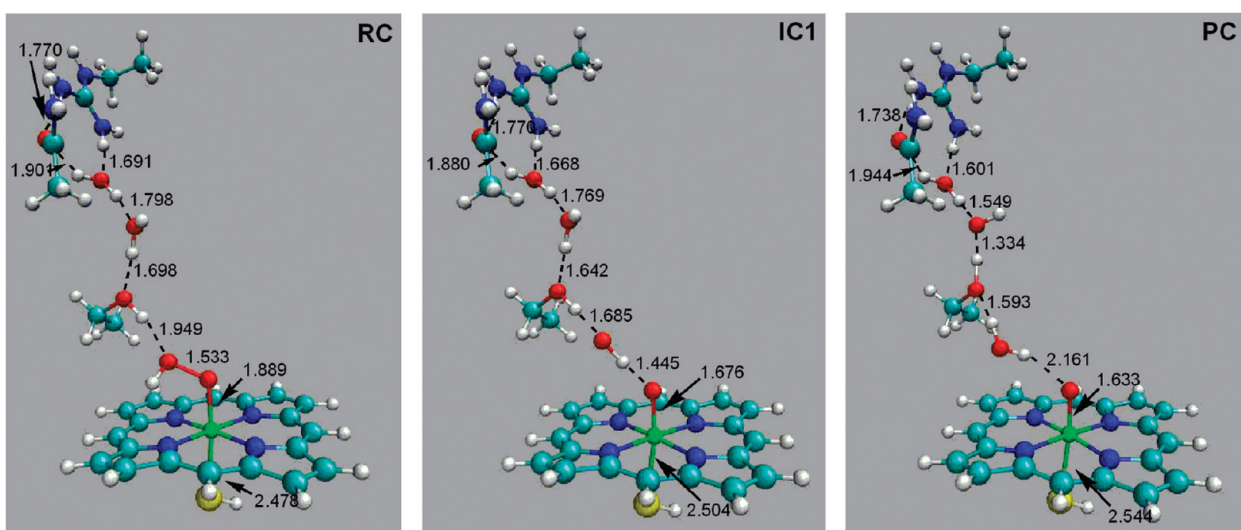


Figure 8. Asn251 mutant, flip model with an extra water and the Arg186 residue included in the QM region: Optimized geometries of Cpd 0, IC1, and PC (UB3LYP/B1/CHARMM). Only the QM region is shown.

network remains intact during 2 ns of classical MD simulation (see Figures S36–S37 and Table S26 in the Supporting Information). This suggests that the formed hydroxide anion may be reprotonated from the bulk solvent by a Grothuss-type

mechanism. It is well-known⁴⁹ that the free energy barriers for such proton transfers are quite low in liquid water, for the migration both of excess protons and of proton holes (involving hydroxide anions),^{49–51} and similarly low barriers have recently

also been reported for the proton transfer along a wirelike water network in bacteriorhodopsin.⁵² We thus consider it likely that such a low-barrier mechanism operates also in our case, but in view of the conformational complexity, we have not attempted to locate any of the corresponding transition states for reprotonation from bulk solvent.

IV. Discussion

In previous QM/MM work,³⁰ we have investigated the first proton transfer in the catalytic cycle of wild-type P450cam and its D251N mutant that leads to the formation of Cpd 0. In the mutant, the Asn251 side chain was found to be flexible in MD simulations and to flip to an orientation away from the active site, thus generating some empty space that can be occupied by an extra water molecule. Participation of this additional water molecule in the hydrogen-bonding network between Arg186/Asn251 and the heme was shown to provide a viable proton-transfer path in the D251N mutant, even though the resulting rate-limiting barrier remained higher than that in the wild-type enzyme.

In the present QM/MM study we address the second proton transfer in the catalytic cycle that converts Cpd 0 into Cpd I. As in the case of wild-type P450cam,¹⁹ we find that the textbook mechanism with initial protonation of the distal oxygen atom of the FeOOH moiety and subsequent heterolytic O–O cleavage does not operate in the mutant. Instead a mixed homolytic–heterolytic mechanism is again more favorable, with initial O–O cleavage followed by proton transfer in the Asp251/Asn251 channel. The initial step is thus the same in both cases, and the corresponding barriers are indeed almost identical in the wild-type enzyme and the D251N mutant (ca. 14 kcal/mol). This is not surprising, since the cleavage of the O–O bond in the FeOOH moiety should not be influenced much by the Asp251/Asn251 replacement.

This substitution does however affect the subsequent proton transfer step. In wild-type P450cam, protonated Asp251 can act as a proton source, and there is a rather facile concerted pathway for proton delivery to the initially formed, hydrogen-bonded OH species. In the D251N mutant, this path requires significant activation according to the current QM/MM calculations for model I (no flip), and it is not available for models II (flip) and III (flip+WatS), where Asn251 does not serve as a proton donor. As in our previous QM/MM work on the first proton transfer,³⁰ the preferred arrangement in the mutant involves a flipped Asn251 conformation with an extra water molecule (WatS) that bridges the Asn251 residue and the crystallographic water molecule (Wat901) close to Thr252. The hydrogen-bonding network thus formed facilitates the second proton transfer, and the corresponding transition state lies indeed only about 12–13 kcal/mol above Cpd 0 (i.e., slightly below the transition state for O–O cleavage). However, the resulting product complex (ca. 7–8 kcal/mol above Cpd 0) still contains an OH anion (Wat901) which cannot be protonated by the Arg186 residue (via WatS). This is in contrast to the mechanism of the first proton transfer in the D251N mutant, where such reprotonation was found to be feasible. We note in this context that the two heme species being protonated in the catalytic cycle differ in their total charge (−2 for the reduced oxyheme complex and −1 for Cpd 0) so that one may expect from general electrostatic arguments that reprotonation from the bulk should be less facile in the case of Cpd 0.

In summary, we have identified one viable path for the second proton transfer in the D251N mutant which terminates at Wat901 and is thus not complete, since it does not provide a route for

reprotonating the formed OH anion (Wat901). We anticipate, however, that reprotonation may be achieved through a water network that connects this OH anion with the bulk solvent. Inspection of the active-site geometry reveals that there is enough space between the residues Arg186, Asn251, and Asn255 to accommodate another water molecule which could form a stable network connecting WatS and Wat149 (at the boundary to the bulk). Classical MD simulations support this idea and reveal that the hydrogen-bonded network remains intact during 2 ns simulations. Proton delivery along such a network via a Grotthuss-type mechanism seems feasible but has not been studied at present.

Experimentally, the D251N mutant catalyzes the hydroxylation of camphor, but it is significantly less active than wild-type P450cam. The observed decrease in the product formation rate by a factor of 30 implies that the rate-limiting barrier should be about 2 kcal/mol higher in the D251N mutant compared with the wild-type enzyme. It is not clear which step in the catalytic cycle is responsible for this reduced activity. Concerning the conversion from Cpd 0 to Cpd I, we find similar barriers for the initial O–O cleavage in both systems, suggesting that the subsequent proton transfer makes the difference. The QM/MM calculations indicate that the active-site proton transfer events are rather facile both in the wild-type enzyme (from Asp251) and in the flip+WatS model of the D251N mutant (from Wat901). It is thus conceivable that a more difficult reprotonation from bulk solvent contributes to the reduced activity of the mutant.

Experimental solvent kinetic isotope effects (SKIEs) provide further mechanistic information. A recent study⁵³ reported an SKIE value (H/D) of 1.8 at 190 K (corresponding roughly to 1.6–1.7 at ambient temperature) for the second proton transfer (Cpd 0 → Cpd I) in wild-type P450cam, indicating some solvent participation in this process. Measurements of the turnover rates in various protium–deuterium mixtures gave SKIE values (H/D) of 1.8 for wild-type P450cam and of 10 for the D251N mutant.¹⁰ These steady-state data do not refer to well-defined elementary reaction steps and can thus not be directly related to our computational results, but the dramatic increase for the D251N mutant suggests that solvent water molecules are more heavily involved in the reactions of this mutant compared with the wild-type enzyme. According to proton inventory analysis, the number of protons involved in the rate-limiting step appears to be far larger in the mutant (five to seven) than in wild-type P450cam.¹⁰ These experimental findings are not at odds with the mechanistic scenario outlined above for the D251N mutant (i.e., proton delivery from bulk solvent to the formed OH anion through a water network).

In general, Cpd 0 can undergo two different protonation reactions, namely coupling (formation of Cpd I and water) and uncoupling (formation of the ferric resting state and hydrogen peroxide). According to the present QM/MM calculations, coupling is favored over uncoupling by a large margin in the D251N mutant. This is consistent with the experimental result that hydroxylation is the dominant reaction also in the D251N mutant, which implies the formation of Cpd I as the crucial reactive species in the P450cam consensus mechanism.

V. Conclusion

The present QM/MM study of the D251N mutant of cytochrome P450cam addresses the mechanism of the protonation reactions involving Cpd 0. The QM/MM calculations were performed at the UB3LYP/CHARMM level with two different

basis sets. For all reactions, only minor differences in the computed relative energies were observed upon basis set extension.

Classical MD simulations indicate that the side chain of the Asn251 residue can adopt two conformations: pointing toward the active site (no flip) and pointing toward the protein surface (flip). The flip of the Asn251 side chain breaks the H-bond network that connects the FeOOH moiety and Asn251, and releases enough space to accommodate an additional water molecule. The stability of the extra water molecule (WatS) was confirmed by MD simulation. Hence, three models were considered for the D251N mutant: no flip, flip, and flip with an extra water molecule.

We investigated two mechanisms that correspond to the formation of Cpd I and water (coupling reaction) and two mechanisms that lead to the formation of hydrogen peroxide and the ferric resting state (uncoupling reaction). The results clearly show, in agreement with experimental⁵⁴ findings, that the uncoupling reaction is unfavorable in the D251N mutant. Likewise, the mechanism that involves initial protonation of Cpd 0 in the coupling reaction is less likely, since the formation of protonated Cpd 0 is difficult. The coupling reaction in the D251N mutant is thus predicted to follow a stepwise mechanism that involves initial cleavage of the O–O bond and subsequent proton transfer to the distal oxygen. As this initial step does not require the participation of a proton source, there is no significant effect due to the D251N mutation.

The course of the subsequent protonation is found to be model-dependent. In model I (no flip), the Asn251 residue serves as the proton source, in spite of its high pK_a value. The first hydrogen transfer has an effective barrier of 20.6 kcal/mol and leads to the formation of Cpd I and deprotonated Thr252, which is then restored in a second step by accepting a proton from Asn251 via Wat901 and an electron from the heme (transition state 24.5 kcal/mol above Cpd 0). The reprotonation of Asn251 is expected to be facile, since Asn251 is in close contact with the bulk solvent.

In model II (flip) the protonation requires three steps. The path is blocked after the protonation of the Thr252 residue, however, since the Asn251 residue does not act as proton source and there is no other proton source in the vicinity. The corresponding product complex lies 19.2 kcal/mol above Cpd 0. Including the Arg186 residue in this model does not help, since it is too far away to enable proton transfer.

In model III (flipped with an extra water molecule in the active site), there is a well-connected H-bond network that facilitates the formation of Cpd I and the reprotonation of Thr252 from Wat901. The proton transfer is effectively concerted with a barrier of around 14 kcal/mol and an endothermicity of 7.7 kcal/mol. The presence of an extra water thus lowers the barrier appreciably and makes model III most realistic. However, we were unable to reprotonate the formed hydroxide anion (Wat901) from Arg186, so that the most likely scenario is reprotonation from the bulk solvent via a water network that remains intact during 2 ns of classical MD simulation. This process has not been studied at the QM/MM level, but it may well require additional activation and thus increase the effective barrier for Cpd I formation.

Acknowledgment. This work was supported by the Max Planck Society.

Supporting Information Available: Energies, spin densities, group charges, and optimized geometries for mechanisms II,

III, and IV. QM/MM energy profiles from pathway calculations. Relative QM/MM energies for mechanism II (with partitioning into QM and MM contributions). MD simulation of the water network in the product complex (mechanism II, model III). Spin densities and group charges of intermediate IC2 in models I and II for different combinations of functional, basis set, and QM region. An overview figure showing all relevant residues. This material is available free of charge via the Internet at <http://pubs.acs.org>.

References and Notes

- (1) Omura, T.; Sato, R. *J. Biol. Chem.* **1962**, *237*, 1375–1376.
- (2) Ortiz de Montellano, P. R. *Cytochrome P450: Structure, Mechanism and Biochemistry*, 3rd ed.; Plenum Press: New York, 2005.
- (3) Schlichting, I.; Berendzen, J.; Chu, K.; Stock, A. M.; Maves, S. A.; Benson, D. E.; Sweet, R. M.; Ringe, D.; Petsko, G. A.; Sligar, S. G. *Science* **2000**, *287*, 1615–1622.
- (4) Poulos, T. L.; Finzel, B. C.; Howard, A. J. *J. Mol. Biol.* **1987**, *195*, 687–700.
- (5) Aikens, J.; Sligar, S. G. *J. Am. Chem. Soc.* **1994**, *116*, 1143–1144.
- (6) Gerber, N. C.; Sligar, S. G. *J. Biol. Chem.* **1994**, *269*, 4260–4266.
- (7) Kamachi, T.; Shiota, Y.; Ohta, T.; Yoshizawa, K. *Bull. Chem. Soc. Jpn.* **2003**, *76*, 721–732.
- (8) Martinis, S. A.; Atkins, W. M.; Stayton, P. S.; Sligar, S. G. *J. Am. Chem. Soc.* **1989**, *111*, 9252–9253.
- (9) Shimada, H.; Makino, R.; Unno, M.; Horiuchi, T.; Ishimura, Y. In *Cytochrome P450cam 8th International Conference*; Libbey, J., Ed.; Eurotext:Paris, 1994, p 299.
- (10) Vidakovic, M.; Sligar, S. G.; Li, H.; Poulos, T. L. *Biochemistry* **1998**, *37*, 9211–9219.
- (11) Guallar, V.; Friesner, R. A. *J. Am. Chem. Soc.* **2004**, *126*, 8501–8508.
- (12) Harris, D. L.; Loew, G. H. *J. Am. Chem. Soc.* **1996**, *118*, 6377–6387.
- (13) Harris, D. L.; Loew, G. H. *J. Am. Chem. Soc.* **1994**, *116*, 11671–11674.
- (14) Sligar, S. G.; Markis, T. M. Private communications, February 2005.
- (15) Gerber, N. C.; Sligar, S. G. *J. Am. Chem. Soc.* **1992**, *114*, 8742–8743.
- (16) Lounnas, V.; Wade, R. C. *Biochemistry* **1997**, *36*, 5402–5417.
- (17) Harris, D. L.; Loew, G. H. *J. Am. Chem. Soc.* **1998**, *120*, 8941–8948.
- (18) Taraphder, S.; Hummer, G. *J. Am. Chem. Soc.* **2003**, *125*, 3931–3940.
- (19) Zheng, J.; Wang, D.; Thiel, W.; Shaik, S. *J. Am. Chem. Soc.* **2006**, *128*, 13204–13215.
- (20) Benson, D. E.; Suslick, K. S.; Sligar, S. G. *Biochemistry* **1997**, *36*, 5104–5107.
- (21) Imai, M.; Shimada, H.; Watanabe, Y.; Matsuhima-Hibiya, Y.; Makino, R.; Koga, H.; Horiuchi, T.; Ishimura, Y. *Proc. Natl. Acad. Sci. U. S. A.* **1989**, *86*, 7823–7827.
- (22) Oprea, T. I.; Hummer, G.; García, A. E. *Proc. Natl. Acad. Sci. U. S. A.* **1997**, *94*, 2133–2138.
- (23) Raag, R.; Martinis, S. A.; Sligar, S. G.; Poulos, T. L. *Biochemistry* **1997**, *36*, 5104–5107.
- (24) Kamachi, T.; Yoshizawa, K. *J. Am. Chem. Soc.* **2003**, *125*, 4652–4661.
- (25) Kumar, D.; Hirao, H.; De Visser, S. P.; Zheng, J.; Wang, D.; Thiel, W.; Shaik, S. *J. Phys. Chem. B* **2005**, *109*, 19946–19951.
- (26) Ogliaro, F.; De Visser, S. P.; Cohen, S.; Sharma, P. K.; Shaik, S. *J. Am. Chem. Soc.* **2002**, *124*, 2806–2817.
- (27) Shaik, S.; Kumar, D.; de Visser, S. P.; Altun, A.; Thiel, W. *Chem. Rev.* **2005**, *105*, 2279–2328.
- (28) Hishiki, T.; Shimada, H.; Nagano, S.; Egawa, T.; Kanamori, Y.; Makino, R.; Park, S. Y.; Adachi, S. I.; Shiro, Y.; Ishimura, Y. *J. Biochem.* **2000**, *128*, 965–974.
- (29) Altarsha, M.; Benighaus, T.; Kumar, D.; Thiel, W. *J. Am. Chem. Soc.* **2009**, *131*, 4755–4763.
- (30) Wang, D.; Zheng, J.; Shaik, S.; Thiel, W. *J. Phys. Chem. B* **2008**, *112*, 5126–5138.
- (31) Altun, A.; Thiel, W. *J. Phys. Chem. B* **2005**, *109*, 1268–1280.
- (32) Schöneboom, J. C.; Lin, H.; Reuter, N.; Thiel, W.; Cohen, S.; Ogliaro, F.; Shaik, S. *J. Am. Chem. Soc.* **2002**, *124*, 8142–8151.
- (33) Schöneboom, J. C.; Thiel, W. *J. Phys. Chem. B* **2004**, *108*, 7468–7478.
- (34) Jorgensen, W. L.; Chandrasekhar, J.; Madura, J. D.; Impey, R. W.; Klein, M. L. *J. Chem. Phys.* **1983**, *79*, 926–935.
- (35) MacKerell, A. D., Jr.; Bashford, D.; Bellott, M.; Dunbrack, R. L., Jr.; Evanseck, J. D.; Field, M. J.; Fischer, S.; Gao, J.; Guo, H.; Ha, S.; Joseph-McCarthy, D.; Kuchnir, L.; Kuczera, K.; Lau, F. T. K.; Mattos, C.,

- Michnick, S.; Ngo, T.; Nguyen, D. T.; Prodhom, B.; Reiher, W. E., III; Roux, B.; Schlenkrich, M.; Smith, J. C.; Stote, R.; Straub, J.; Watanabe, M.; Wiórkiewicz-Kuczera, J.; Yin, D.; Karplus, M. *J. Phys. Chem. B* **1998**, *102*, 3586–3616.
(36) Brooks, B. R.; Bruccoleri, R. E.; Olafson, B. D.; States, D. J.; Swaminathan, S.; Karplus, M. *J. Comput. Chem.* **1983**, *4*, 187–217.
(37) Becke, A. D. *J. Chem. Phys.* **1993**, *98*, 5648–5652.
(38) Hay, P. J.; Wadt, W. R. *J. Chem. Phys.* **1985**, *82*, 299–310.
(39) Hehre, W. J.; Ditchfield, K.; Pople, J. A. *J. Chem. Phys.* **1972**, *56*, 2257–2261.
(40) Schäfer, A.; Horn, H.; Ahlrichs, R. *J. Chem. Phys.* **1992**, *97*, 2571–2577.
(41) Schäfer, A.; Huber, C.; Ahlrichs, R. *J. Chem. Phys.* **1994**, *100*, 5829–5835.
(42) Smith, W.; Forester, T. R. *J. Mol. Graphics* **1996**, *14*, 136–141.
(43) Sherwood, P.; De Vries, A. H.; Guest, M. F.; Schreckenbach, G.; Catlow, C. R. A.; French, S. A.; Sokol, A. A.; Bromley, S. T.; Thiel, W.; Turner, A. J.; Billeter, S.; Terstegen, F.; Thiel, S.; Kendrick, J.; Rogers, S. C.; Casci, J.; Watson, M.; King, F.; Karlsen, E.; Sjøvoll, M.; Fahmi, A.; Schäfer, A.; Lennartz, C. *THEOCHEM* **2003**, *632*, 1–28.
(44) Ahlrichs, R.; Bär, M.; Häser, M.; Horn, H.; Kälmel, C. *Chem. Phys. Lett.* **1989**, *162*, 165–169.
(45) Billeter, S. R.; Turner, A. J.; Thiel, W. *Phys. Chem. Chem. Phys.* **2000**, *2*, 2177–2186.
(46) Bakowies, D.; Thiel, W. *J. Phys. Chem.* **1996**, *100*, 10580–10594.
(47) Sherwood, P.; De Vries, A. H.; Collins, S. J.; Greatbanks, S. P.; Burton, N. A.; Vincent, M. A.; Hillier, I. H. *Faraday Discuss.* **1997**, *106*, 79–92.
(48) Nagano, S.; Poulos, T. L. *J. Biol. Chem.* **2005**, *280*, 31659–31663.
(49) Marx, D. *ChemPhysChem* **2006**, *7*, 1848–1870.
(50) Muller, R. P.; Warshel, A. *J. Phys. Chem.* **1995**, *99*, 17516–17524.
(51) Tuckerman, M. E.; Chandra, A.; Marx, D. *Acc. Chem. Res.* **2006**, *39*, 151–158.
(52) Mathias, G.; Marx, D. *Proc. Natl. Acad. Sci. U. S. A.* **2007**, *104*, 6980–6985.
(53) Kim, S. H.; Yang, T.-C.; Perera, R.; Jin, S.; Bryson, T. A.; Sono, M.; Davydov, R.; Dawson, J. H.; Hoffman, B. M. *Dalton Trans.* **2005**, 3464–3469.
(54) Markis, T. M.; Denisov, I. G.; Schlichting, I.; Sligar, S. G. In *Cytochrome P450: Structure, Mechanism and Biochemistry*, 2nd ed.; Plenum Press: New York, 1995.

JP809838K